Journal of Catalysis 272 (2010) 92–100

Contents lists available at ScienceDirect

Journal of Catalysis

journal homepage: www.elsevier.com/locate/jcat

Sol–gel-entrapped nano silver catalysts-correlation between active silver species and catalytic behavior

Vasile I. Pârvulescu [a,*], Bogdan Cojocaru [a], Viorica Pârvulescu [b], Ryan Richards [c,**], Zhi Li [c], Chris Cadigan [c], Pascal Granger [d,***], Pierre Miquel [d], Chris Hardacre [e,****]

[a] Department of Chemical Technology and Catalysis, University of Bucharest, B-dul Regina Elisabeta 4-12, Bucharest 030016, Romania
[b] Institute of Physical Chemistry of the Romanian Academy, Splaiul Independentei St. 202, P.O. Box 194, Bucharest 060021, Romania
[c] Department of Chemistry and Geochemistry, Colorado School of Mines, Golden, CO 80401, USA
[d] Unité de Catalyse et de Chimie du Solide, UMR CNRS 8181, Université de Lille1, Bâtiment C3, 59650 Villeneuve d'Ascq, France
[e] School of Chemistry and Chemical Engineering, Queen's University, David Keir Building, Stranmillis Road, Belfast BT9 5AG, UK

ARTICLE INFO

Article history:
Received 6 January 2010
Revised 17 February 2010
Accepted 7 March 2010
Available online 13 April 2010

Keywords:
Silver colloids
Sol–gel synthesis
NO reduction with hydrogen and CO

ABSTRACT

Silver colloids prepared by reducing $AgNO_3$ in aqueous solution with sodium citrate were embedded in alumina following two different preparation procedures resulting in samples containing 3 and 5 wt.% silver. Characterization of these materials using TEM, XPS, XAES, CP/MAS NMR, XRD, and adsorption–desorption isotherms of nitrogen showed that embedding the pre-prepared silver colloids into the alumina via the sol–gel procedure preserved the particle size of silver. However, as XAES demonstrates, the catalysts prepared in a sol–gel with a lower amount of water led to embedded colloids with a higher population of Ag^+ species. The catalytic behaviors of the resultant catalysts were well correlated with the concentration of these species. Thus, the active silver species of the catalysts containing more Ag^+ species selectively converts NO to N_2. However, subsequent thermal aging leads to an enhancement of the conversion of NO parallel to slight alteration of the selectivity with the appearance of low amounts of N_2O despite an increase of Ag^+ species. Accordingly, an optimal surface Ag^0/Ag^+ ratio is probably needed, independently of the size of silver particles. It was found that this optimal ratio strongly depends on the operating conditions during the synthesis route.

1. Introduction

Catalysis with silver nanoparticles has received special attention recently due to the efficiency demonstrated by these systems in developing new catalysts for a wide variety of reactions, such as hydrogenation [1], oxidation [2], and environmental applications [3].

The deposition of the silver nanoparticles was performed on various supports such as carbon-derived materials [4], Si nanowire arrays [5], hydrotalcite [6], and silica in different forms (colloidal [7], porous [8], spheres [9], MCM-41 [10]) using different methodologies. Although the particles remained nanoscale in size, in many of these reports, multimodal particle size distributions resulted after the deposition of silver. Reports on the use of such colloids stabilized in different polymeric structures such as poly(N-isopropylacrylamide) [11] or poly(vinylpyrrolidone) [12] have been presented as well, but only for reactions carried out at low temperatures.

Silver-supported alumina catalysts have been investigated as well. The preparation of these catalysts was performed either by impregnation of the metal salts [13], precipitation and modified precipitation [14], or water–alcohol and micro-emulsion methods [14,15]. The sol–gel technique has also been used, but the introduction of silver was carried out from a dispersion of a silver salt in the pre-synthesized gel [16]. Similar to the other supports, the use of this preparation led to silver particles with nanometer sizes but with a broad size distribution.

There are many papers reporting that the deposition of silver on alumina provides active catalysts for SCR deNO_x processes under lean conditions. In the presence of excess oxygen [17], some of these studies stipulated that in this process the sample mean particle size or particle size distribution alone could not explain the large differences observed in the catalytic activity [18]. It was found that in this process hydrogen had a remarkable effect on the temperature range over which NO_x could be reduced during the SCR reaction with octane [19]. Further studies, based on *in-situ* EXAFS measurements suggested the effect of hydrogen is a

* Corresponding author. Fax: +4 0 21 410 02 41.
** Corresponding author. Fax: +1 303 273 3629.
*** Corresponding author. Fax: +33 0 32043 6561.
**** Corresponding author. Fax: +44 0 28 9097 6524.
E-mail addresses: vasile.parvulescu@g.unibuc.ro (V.I. Pârvulescu), rrichard@mines.edu (R. Richards), pascal.granger@univ-lille1.fr (P. Granger), c.hardacre@qub.ac.uk (C. Hardacre).

0021-9517/$ - see front matter © 2010 Elsevier Inc. All rights reserved.
doi:10.1016/j.jcat.2010.03.008

chemical one and not the result of a change in the structure of the active site [20]. Some of these results and their effect on silver in these reactions have been reviewed by Burch et al. [21].

The aim of this study was to prepare nano-embedded Ag/Al_2O_3 catalysts using a colloid approach in combination with a sol–gel synthesis route and to characterize the thermal resistance of those embedded catalysts under reactive conditions in wet atmosphere on the basis of earlier investigations which reported a gradual increase in activity in the presence of water probably related to structural changes [22,23]. In this respect, the materials were characterized both as freshly-prepared and used catalysts using a multitude of techniques: TEM, XPS, XAES, CP/MAS NMR, XRD, adsorption–desorption isotherms of nitrogen, etc. Particular attention has been paid to changes in surface properties and related catalytic performance in the reduction of NO by hydrocarbons (propene and decane) under real exhaust gas conditions. It has been found that the extent of surface reconstructions, which may occur under running conditions at high temperature, is probably driven by the surface properties of the as-prepared catalysts, i.e. to the preparation route.

2. Materials and methods

2.1. Catalyst preparation and characterization

Silver colloids were prepared by reducing $AgNO_3$ in an aqueous solution. In a typical preparation, 0.294 g sodium citrate was added to 50 cm^3 of 10 mM $AgNO_3$ aqueous solution in an ice bath. $NaBH_4$ (0.019 g) was added to the solution at once with strong stirring and a black powder formed in solution. The solution was then filtered and dried at room temperature under vacuum.

The catalysts were prepared from 98.5 g aluminum butoxide ($Al(OBu)_3$) dissolved in isobutanol (150 cm^3) which was subsequently added to an isobutanol (90 cm^3) solution of 17.2 g Pluronic 84 ($(EO)_{19}(PO)_{39}(EO)_{19}$) which acted as the surfactant. The resulting mixture was then heated to 70 °C for 6 h. Water was added, and the reaction was maintained at 80 °C for 10 h followed by 100 °C for 20 h. The Ag colloid dissolved in water was added to this mixture under vigorous stirring. The samples were preserved at room temperature for 48 h, dried under vacuum at 110 °C, and then calcined at 500 °C with a slope of 0.5 °C min^{-1}. The Ag content was confirmed by ICP-AES analysis. This preparation yielded the following samples: 13-AlAg, containing 3 wt.% Ag, when the molar ratio alkoxide:alcohol:water was of 1:10:25, 23-AlAg and 25-AlAg, containing 3 and 5 wt.% Ag, respectively, when the molar ratio alkoxide:alcohol:water was of 1:5:10.

2.2. Catalyst characterization

The prepared catalysts were characterized *ex-situ* by BET nitrogen physisorption at −196 °C (Surface area and pore size values were calculated from nitrogen adsorption–desorption isotherms recorded on a Micromeritics ASAP-2010 automated instrument. Calcined samples were degassed for 15 h at 403 K and 10^{-6} Torr before analysis. Surface areas were estimated according to the BET model, and pore size dimensions were calculated using the BJH method.), powder X-ray diffraction (XRD) (Shimadzu XRD-7000 with Cu Kα (λ = 1.5418 Å, 40 kV, 40 mA) radiation at a scanning rate of 0.10 min^{-1} in the 2Θ range of 10–80°), transmission electron microscopy, XPS, XAES, and CP/MAS ^{27}Al NMR spectroscopy. Transmission electron microscopy (TEM) was carried out with a JEOL JEM-1010 instrument operating at 100 kV. X-ray photoelectron spectroscopy (XPS) and Auger electron spectroscopy (XAES) experiments were performed by using a Specs GmbH setup. The excitation was done by using a conventional dual anode X-ray source (Specs XR 50) using the Mg K alpha line (1253.6 eV). The sample consisted in powder dispersed on two-sided adhesive tape. In order to compensate for charging, a flood gun (Specs FG 20) was employed, operating at 3 V and 0.3 mA. Photolectrons and Auger electrons are analyzed by using a (Specs) Phoibos 150 hemispherical analyzer, with estimated resolution (FWHM) of 0.85 eV at 12 eV pass energy on Ag 3d core levels excited with Mg K alpha. For the actual experiments, a pass energy of 30 eV (estimated resolution: 1.3 eV FWHM) was employed for the core levels and 50 eV for survey scans, including the Auger electrons. 27Al MAS-NMR spectra were recorded at room temperature on MAS-NMR Avance 400 Bruker spectrometer, at 104.2 MHz, in a 9.4 T field, with 15 kHz spinning rate, using $Al(NO_3)_3$ water solution as reference. Deconvolution of the CP/MAS-NMR spectra was carried out using the DMFIT program [24].

2.3. Catalytic performances

Catalytic performances were evaluated from temperature-programmed reduction (TPR) of NO by hydrocarbons (propene and decane) in the presence of CO and H_2 according to the following experimental conditions: 300 ppm NO, 900 ppm (C) propene, 300 ppm CO, 1000 ppm (C) decane, 2000 ppm H_2, 10 vol.% O_2, 10 vol.% CO_2, 5 vol.% H_2O, W/F_0 = 0.072 g s cm^{-3}. Prior to the reaction, all catalyst samples were submitted to a pre-activation thermal treatment under flowing helium at 400 °C. The experimental procedure, illustrated in Fig. 1, was adopted for evaluating catalytic performances. As shown, freshly-prepared catalysts were submitted to preliminary TPR1 from 75 to 500 °C with a heating rate dT/dt = 2 °C min^{-1}, then catalyst samples were maintained overnight in isothermal conditions under reactive atmosphere. After cooling down at room temperature, successive temperature-programmed experiments were achieved on aged samples (TPR2).

Reactants and products were analyzed using a two column Varian micro-chromatograph CP4900 each fitted with a thermal conductivity detector. NO, CO, N_2, and O_2 were separated on a molecular sieve 5A column whereas N_2O, CO_2, and propene were separated on a Porapak Q column. The overall conversion of NO_x was checked using a Beckman 951A NO/NO_x chemiluminescence analyzer. The overall consumption of H_2 and decane was quantified using a Balzer quadrupole mass spectrometer (Omnistar GSD 301).

The overall conversion X_i of the reactant i (with i = NO_x, CO, H_2, C_3H_6, decane) was calculated according to the following Eq. (1) where F_i stands for the molar flow rate of the reactant i.

$$X_i = \frac{F_{i,0} - F_i}{F_{i,0}} \tag{1}$$

The conversion of NO into N_2 and N_2O ($X_{NO,red}$) and the selectivity toward the production of nitrogen S_{N_2} were calculated according to Eqs. (2) and (3), respectively:

$$X_{NO,red} = X_{NO\rightarrow N_2} + X_{NO\rightarrow N_2O} = \frac{2F_{N_2} + 2F_{N_2O}}{F_{NO,0}} \tag{2}$$

$$S_{N_2} = \frac{r_{NO\rightarrow N_2}}{r_{NO\rightarrow N_2} + r_{NO\rightarrow N_2O}} = \frac{X_{NO\rightarrow N_2}}{X_{NO\rightarrow N_2} + X_{NO\rightarrow N_2O}} \tag{3}$$

3. Results and discussion

3.1. Physio-chemical characterization of bulk and surface properties

Table 1 compiles the textural characteristics of the investigated materials. As for the pure alumina support, the procedure with the gel composition: molar ratio alkoxide:alcohol:water of 1:10:25 led to a material with a high specific surface area, high pore volume,

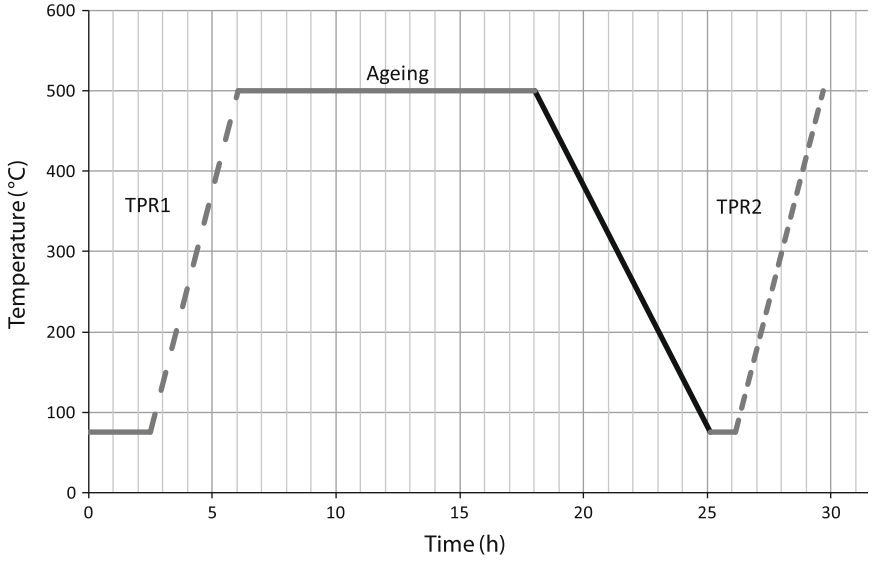

Fig. 1. Experimental protocol used for the evaluation of the catalytic performances of silver-based catalysts.

Table 1
Textural characteristics of the investigated materials.

Sample	Ag content (wt.%)	BET surface area ($m^2\ g^{-1}$)	Pore volume ($cm^3\ g^{-1}$)	Pore size (nm)
AlM1	0	524	1.02	Monomodal, 7.5
13-AlAg	3	408	0.97	Monomodal, 7.5
23-AlAg	3	333	0.68	Bimodal, 3 + 7.5
25-AlAg	5	336	0.58	Bimodal, 3 + 6

and a monomodal pore size distribution. Changing the gel composition to molar ratio alkoxide:alcohol:water of 1:5:10 led to materials with smaller surface areas and pore volumes exhibiting bimodal pore size distributions. In agreement with the *t*-plot values, the presence of micropores is insignificant for both preparation routes.

Increasing the metal loading exhibited only a slight influence on the pore volume and pore size. A small decrease in the pore volume has been observed after increasing the metal concentration to 5 wt.%. Surprisingly, only the largest pore size diameter seems to be significantly affected. Thus, for the 2-AlAg series, the pore size distribution remained bimodal, but the size of the larger pores shifted from 7.5 nm to 6 nm.

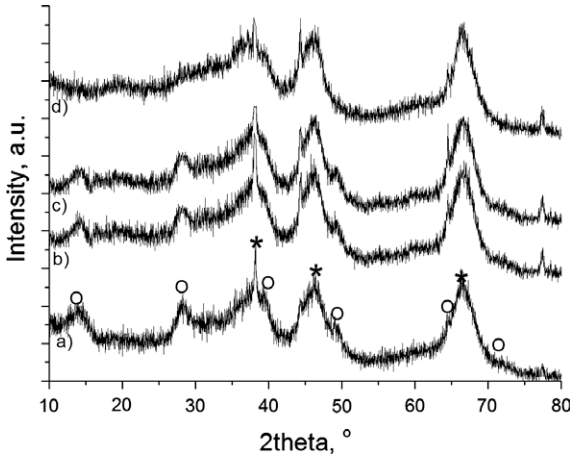

Fig. 2. XRD patterns of the investigated samples: (a) fresh 13-AgAl, (b) fresh 23-AgAl, (c) aged 23-AgAl, and (d) 25-AgAl (o-γ-Al_2O_3 phase, x-Ag^0 phase).

Fig. 2 shows the XRD patterns of the fresh investigated samples. These patterns exhibit broad X-ray lines assigned to amorphous γ-Al_2O_3 phase and lines at 2Θ 37, 47, and 67 due to metallic silver particles. While the intensities of lines assigned to silver have very similar intensities, the peaks caused by alumina exhibit a low intensity in the case of the 13-AgAl catalyst. This demonstrates that using this procedure neither the concentration of the silver colloids introduced in the preparation of the samples nor the change in the gel composition in the preparation procedure is generating changes in the structure of silver particles.

The XRD analyses of these samples after they have been investigated in the TPR of NO by hydrocarbons (propene and decane) in the presence of CO and H_2 did not suggest structural changes, indicating that these structures are highly stable irrespective of the nature of the atmosphere (either oxidative or reductive conditions) and at temperatures as high as those released during the combustion of the different hydrocarbons or even CO and hydrogen on the catalyst surface. No bulk oxidation of silver 25-AlAg seems to occur after exposure to lean conditions at high temperature. ^{27}Al MAS-NMR analysis showed some differences among the synthesized samples (Fig. 3). The ^{27}Al MAS-NMR spectrum of the sol–gel-synthesized alumina following the described procedure indicated only one line located at around 13 ppm that corresponds to hexacoordinated aluminum. The introduction of the silver colloids changed the patterns of these spectra, and a second line appears at 74–76 ppm that is generally assigned to tetracoordinated aluminum [25]. It is also important to note the changes induced by the gel composition in the ^{27}Al MAS-NMR spectra of these samples. Thus, the chemical shift assigned to the tetracoordinated aluminum species tends toward higher values on 2-AlAg compared to 1-AlAg samples which might be related to slight distorsion on tetracoordinated aluminum sites due to Ag species incorporation. A remaining questioning point, correlated to those structural changes, could be the induced-effect on the acidic properties of AgAl catalysts. This observation might have some repercussions on the catalytic properties as previous suggested on the formation of ad-NO_x species on the support [26]. This behavior may allow us to speculate that silver interacts with tetracoordinated aluminum sites. This interac-

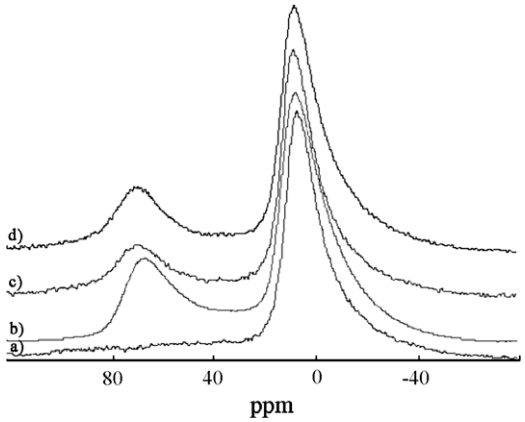

Fig. 3. ^{27}Al MAS-NMR spectra of the supported silver-based catalysts samples: (a) Al_2O_3, (b) 13-AgAl, (c) 23-AgAl, and (d) 25-AgAl.

tion may also be responsible for the changes that occurred in the texture of the catalysts when the silver loading had been increased from 3 to 5 wt.%.

TEM analysis of 13-AgAl and 23-AgAl is presented in Fig. 4. Due to the resolution limit of the instrument and the low contrast caused by the amorphous structure of alumina, the tiny silver particles cannot be clearly distinguished from Fig. 4. However, some dark spots around 3–5 nm can be observed, which could be silver particles since silver has a higher electron density than alumina. The amorphous alumina of both samples show similar fiber-like texture. However, the alumina fiber in 13-AgAl is better organized than that in 23-AgAl and therefore, 13-AgAl gives a larger pore volume and uniform pore size, which agrees well with BET data. No difference in the size of the silver particles and surface morphology was observed for 23-AgAl and 25-AgAl catalysts.

In addition to particle size and crystallinity, the oxidation state of the metal nanoparticles is another very important factor controlling the catalytic behavior of these materials. XPS analyses led to the results presented in Fig. 5B and Table 2. B.E. values have been corrected using the usual reference value of the Al 2p core level in alumina of 74.6 eV. Previous XPS investigations reported B.E. values of 367.4 and 367.8 eV for AgO and Ag_2O, respectively, whereas current values for metallic silver clusters are usually located at 368.0 eV [27]. B.E. values recorded on as-prepared and aged 13 and 23-Ag/Al_2O_3 seem more in agreement with current values recorded on metallic Ag particles [28]. No significant change in spectral features seems to occur after thermal aging, except on 23-Ag/Al_2O_3 with a shift from 368.8 to 368.2 eV which could reflect an increase of relative concentration of electrophilic silver species in the depth analyzed by XPS (5–10 nm). Such a tendency could drive the catalytic performances in the light of previous investigations [29] which suggest a significant enhancement on the selective reduction of NO by hydrocarbon at the expense of the catalytic combustion of unburned hydrocarbons on $Ag_n^{\delta+}$ clusters while the opposite trend is observable on metallic silver particles. Indeed, a wide number of publications emphasized the fact that the atomic Ag^0/Ag^+ ratio is the driving force in determining the performances in the reduction of NO to nitrogen [30]. Changing the molar composition during the embedding process does not influence significantly the B.E. values. It is also remarkable that the atomic Ag/Al ratio does not vary after thermal aging, highlighting the high stability of silver-based catalysts with no significant particle sintering during exposure at 500 °C under running conditions. Such a tendency differs from that earlier reported on Ag/SiO_2–TiO_2 samples showing a significant increase of the surface Ag/Si ratio with an increase in the metal loading and after reaction ascribed to the aggregation

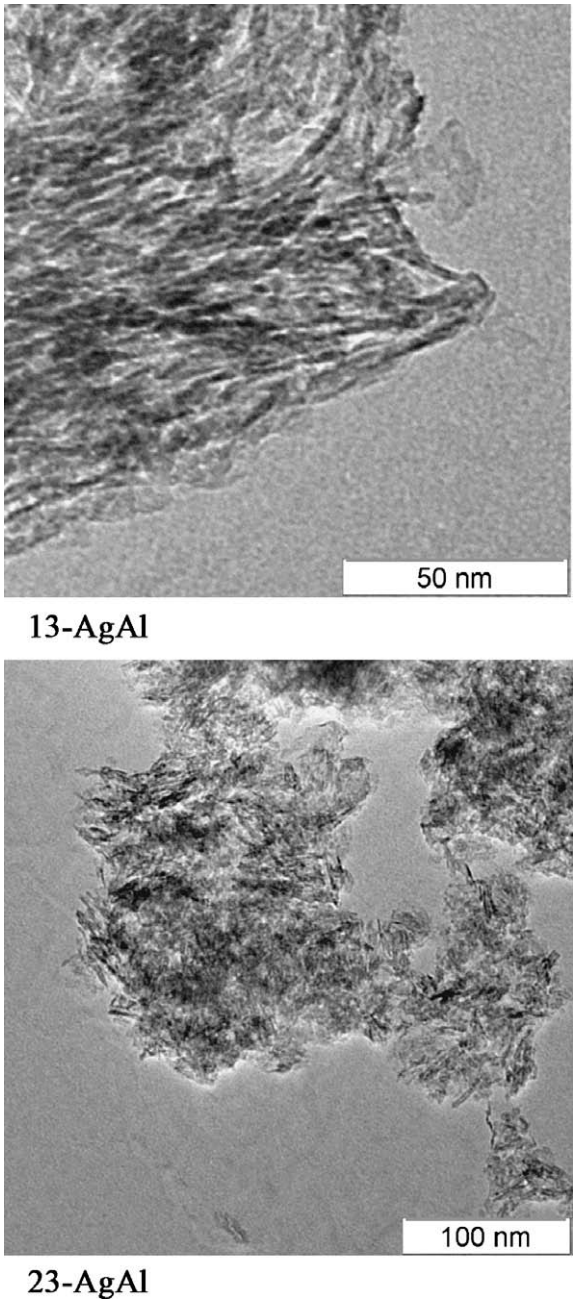

Fig. 4. TEM pictures of the 13-AgAl and 23-AgAl samples.

of Ag species [31]. Regarding 13- and 23-Ag/Al_2O_3, both exhibit similar spectral features. An additional important observation revealed by XPS measurements is related to the weak detection of N-containing species on the Ag1 catalyst (binding energy of the N1s species located at 398.7 eV) while no nitrogen species were detected for the AlAg2 series after reaction. Nitrate/nitrite species usually appear at 407 and 404 eV, respectively, but are not observed here. The XPS signal at 398.7 (Fig. 6) is assigned to chemisorbed N atoms, and/or N-containing species, which account for the lower oxidation state of nitrogen [32].

On the basis of XPS observation, it seems reasonable to infer that formed alumina is providing a very effective protecting shell. The exposure of the catalysts to the reaction conditions does not change either the oxidation state of the nanoparticles or the relative surface concentration of the metal. Such a trend is in relatively

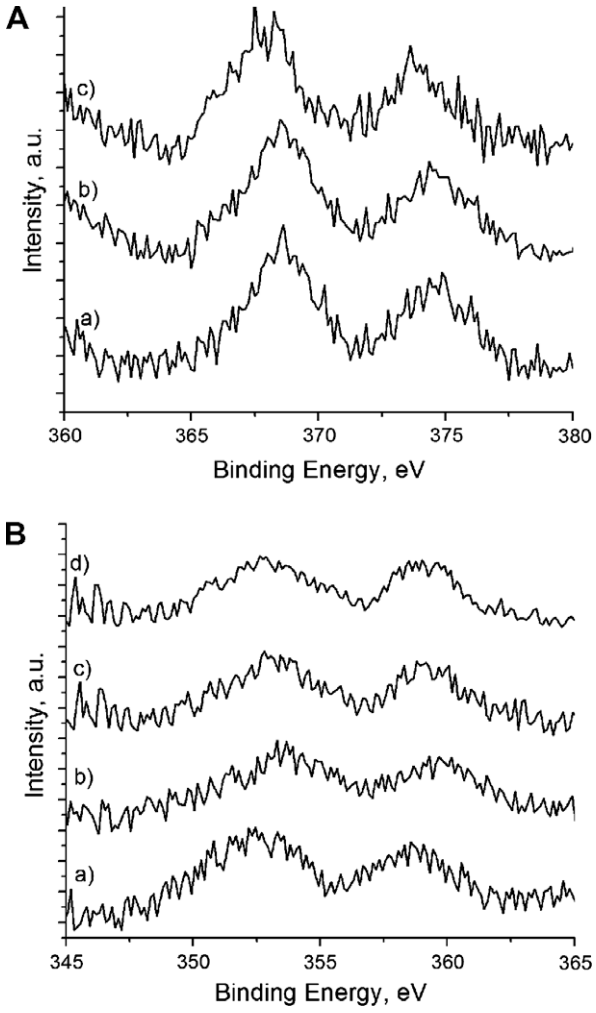

Fig. 5. Ag MNN XAES spectra (A): (a) 23-AlAg, (b) 25-AlAg, and (c) 13-AlAg, and XPS spectra (B) in the region of Ag 3d level for the fresh: (a) 13-AlAg, (b) 23-AlAg, and (c) 25-AlAg, and used catalysts: (d) 25-AlAg.

Table 2
XPS parameters of the investigated materials.

Sample	Binding energy (eV)			Atomic Ag/Al ratio × 10^3	
	Ag $3d_{5/2}$	Ag MNN	O 1s	XPS	bulk
13-AlAg fresh	369.0	352.0	531.6	16.1	5.85
13-AlAg aged	368.6	352.3	532.0	16.2	5.83
23-AlAg fresh	368.8	353.1	532.0	15.4	5.74
23-AlAg aged	368.2	353.4	532.0	14.4	5.79
25-AlAg fresh	368.9	352.7	531.9	17.0	9.81
25-AlAg aged	368.9	352.9	531.6	20.8	9.84

good agreement with TEM and XRD observations, but also with the textural characterization that showed 2-AlAg samples exhibit a surface area that is 20% smaller than that of the 1-AlAg sample. Additional XPS observations on aged samples do not reveal changes on the surface composition emphasizing a relative good stability during thermal aging. This observed behavior is corroborated by the measurements of Ag MNN spectrum. Recently, it was indicated that the precise chemical state of silver could be more easily discriminated by the peak position of XAES, which is more sensitive to the chemical environment than XPS, especially when the corresponding core-level XPS spectra are insensitive to different chemical states [31]. According to this literature report, it appears that the small silver particles indeed possess Ag^+ ions.

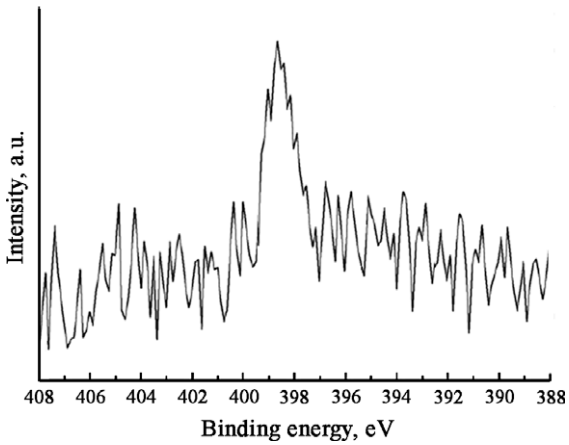

Fig. 6. N1s XPS spectrum of the 13-AgAl catalyst after the catalytic tests.

However, the population of these species seems to be influenced by the preparation procedure. The binding energy of the Ag MNN species for the 23-Ag/Al_2O_3 samples is almost 1 eV higher than that of 13-Ag/Al_2O_3, indicating an increased population of the Ag^+ ions in these catalysts (Fig. 5A and Table 2). The XAES results also confirm the protecting effect of the support mentioned above and seem in rather good agreement with previous tendencies related to the deviation observed on B.E. values of the Ag $3d_{5/2}$ core level. The difference between the fresh and the tested catalyst exceeds 0.5 eV only for the sample containing 5 wt.% Ag.

3.2. Catalytic behavior of supported Ag-based catalysts: tentative correlations between surface and catalytic properties

According to the following set of equations, the target reaction is the reduction of NO to nitrogen which competes with the formation of side products such as N_2O.

$$2NO + 2CO = CO_2 + N_2 \quad (4)$$
$$2NO + 2H_2 = H_2O + N_2 \quad (5)$$
$$2NO + C_xH_y = CO_2 + H_2O + N_2 \quad (6)$$
$$2NO + H_2 = H_2O + N_2O \quad (7)$$

Oxidation reactions under lean conditions (excess of oxygen) usually compete and might considerably alter the selectivity.

$$2NO + O_2 = 2NO_2 \quad (8)$$
$$2H_2 + O_2 = 2H_2O \quad (9)$$
$$C_xH_y + O_2 = CO_2 + H_2O \quad (10)$$
$$2CO + O_2 = 2CO_2 \quad (11)$$

Let us note that the oxidation of NO to NO_2, which is thermodynamically favorable at low temperature, might lead to the stabilization of nitrate species which can induce significant loss of activity at low temperature by a poisoning effect. Subsequently, reaction processes associated with these species decomposition and/or direct interaction with the reducing agent might also cause interference during temperature-programmed experiments.

3.2.1. 13-Ag/Al_2O_3 catalyst

TPR1 recorded on 13-Ag/Al_2O_3 is illustrated in Fig. 7. As shown, the conversion of NO to N_2 and N_2O, calculated according to Eq. (2), starts above 180 °C but is abnormally low with a 12% maximum in the temperature range 180–500 °C. Further, some discrepancies arise in comparison with the overall NO conversion calculated from the chemiluminescence analyzer according to Eq. (1). As observed, they do not coincide and the unexpected negative values

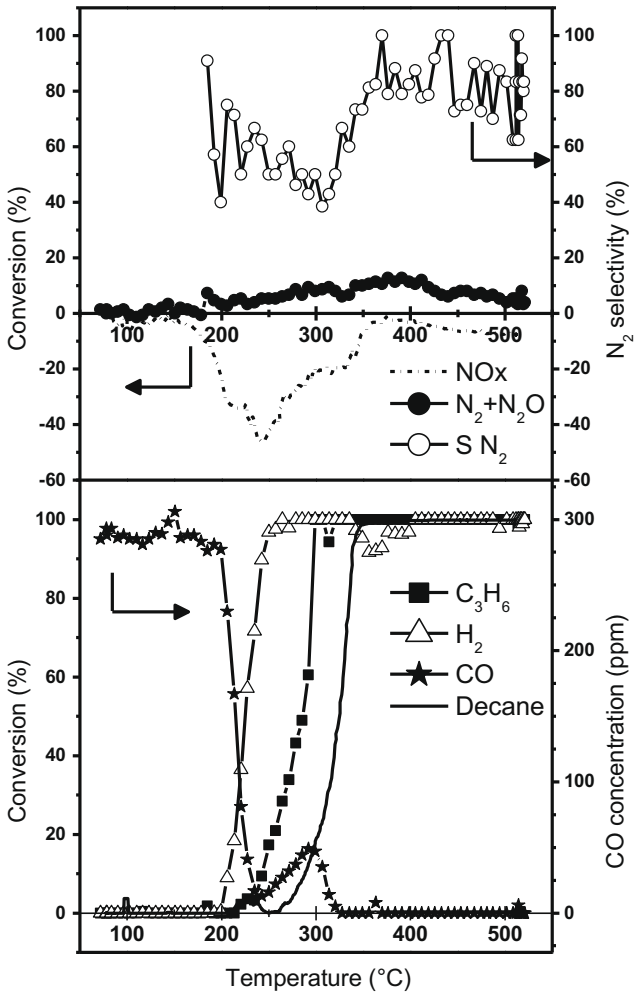

Fig. 7. Temperature-programmed reduction of NO by hydrocarbons (TPR1) on 13-Ag/Al_2O_3 (reaction conditions: 300 ppm NO, 300 ppm CO 900 ppmC C_3H_6, 1000 ppmC Décane, 2000 ppm H_2, 10 vol.% O_2, 10 vol.% CO_2, 5 vol.% H_2O – $W/F_0 = 0.072$ g s cm^{-3}).

reflect an extra NO formation which takes place possibly from the direct decomposition of stored nitrates and/or subsequent reduction of ad-NO_x species by the reducing agents yielding gaseous NO. The selectivity profile S_{N_2} vs. temperature reveals two selectivity regimes. As illustrated in Fig. 7, a low temperature selectivity range is observable below 300 °C with a gradual decrease of S_{N_2} from 91% to 38.5% with an increase in temperature. On the other hand, a discontinuity is observable above 300 °C, with a reverse tendency, S_{N_2} increasing significantly in this temperature range and then stabilizing at ≈80%.

Let us now examine the overall conversion of the reducing agents. The conversion of H_2 and CO occurs more readily than that of propene and decane starting at 200 °C and then being quasi-complete up to 240 °C, whereas the conversion of propene and decane, starting, respectively, at 223 and 250 °C, becomes complete up to 300 °C. The following activity sequence can be qualitatively established based on the light-off temperature, T_{50} (temperature corresponding to 50% conversion of the compound (i): CO (T_{50} = 221 °C) > H_2 (T_{50} = 227 °C) > C_3H_6 (T_{50} = 292 °C) > $C_{10}H_{22}$ (T_{50} = 325 °C). Two conversion ranges are distinguishable for CO with a minimum located at 292 °C. The presence of this minimum might reflect different phenomena occurring under reaction conditions. Generally speaking, CO oxidation by O_2 is catalyzed by metallic silver clusters. The fact that oxidation reactions preferentially take place on 13-Ag/Al_2O_3 is in relative good agreement with surface characterization indicating the predominant metallic character of Ag particles with a lower amount of Ag^+ species than on 23-Ag/Al_2O_3.

TPR2 recorded after isothermal aging overnight at 500 °C does not reveal significant changes with respect to the conversion of NO_x with very low values in the temperature range of the study (Fig. 8). The light-off temperatures for the conversion of H_2, propene, and CO shift to higher temperature except that of decane. In this latter case, a low temperature conversion range develops between 180 and 280 °C. In the light of those results, thermal aging under running conditions seems to have a detrimental effect on the oxidative properties of 13-Ag/Al_2O_3 but no parallel development in the selective conversion of NO_x to nitrogen is discernible.

3.2.2. 23- and 25-Ag/Al_2O_3 catalysts

Clearly, 23-Ag/Al_2O_3 behaves differently as is well-illustrated in TPR1 in Fig. 9. As shown, 23-Ag/Al_2O_3 converts NO at higher temperature than on 13-Ag/Al_2O_3 (333 °C vs. 180 °C) but to a larger extent, a maximum NO conversion of 24–27% is attained in the temperature range 345–410 °C and then gradually decreases at higher temperature reaching 8% at 500 °C. It is worthwhile to note that NO is selectively converted into N_2, contrary to 13-Ag/Al_2O_3. Subsequent comparison of NO_x conversion values calculated from gas chromatography and chemiluminescence analyses does not

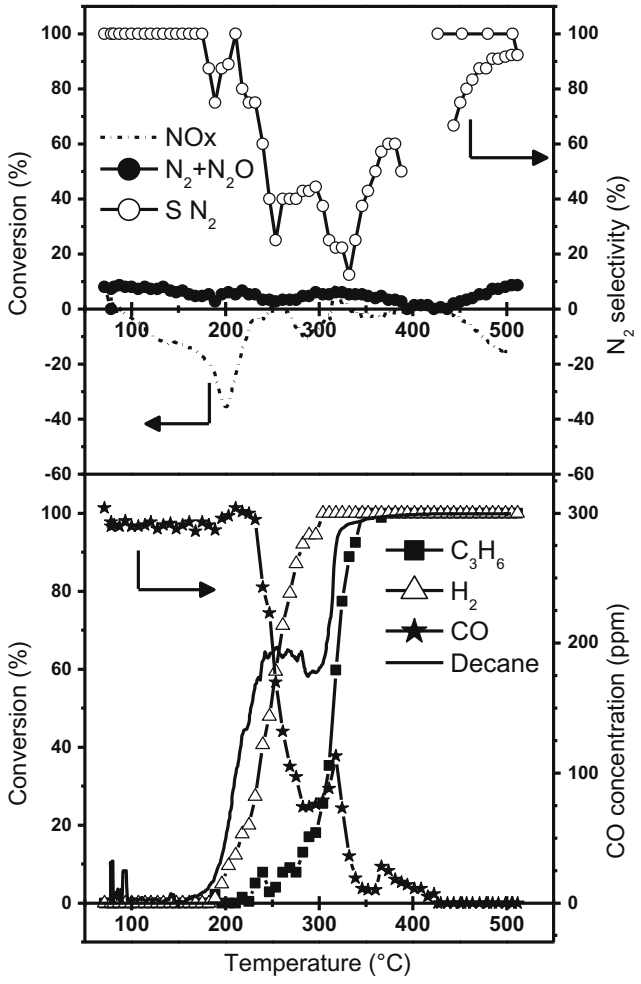

Fig. 8. Temperature-programmed reduction of NO by hydrocarbons (TPR2) on 13-Ag/Al_2O_3 (reaction conditions: 300 ppm NO, 300 ppm CO 900 ppmC C_3H_6, 1000 ppmC Decane, 2000 ppm H_2, 10 vol.% O_2, 10 vol.% CO_2, 5 vol.% H_2O – $W/F_0 = 0.072$ g s cm^{-3}).

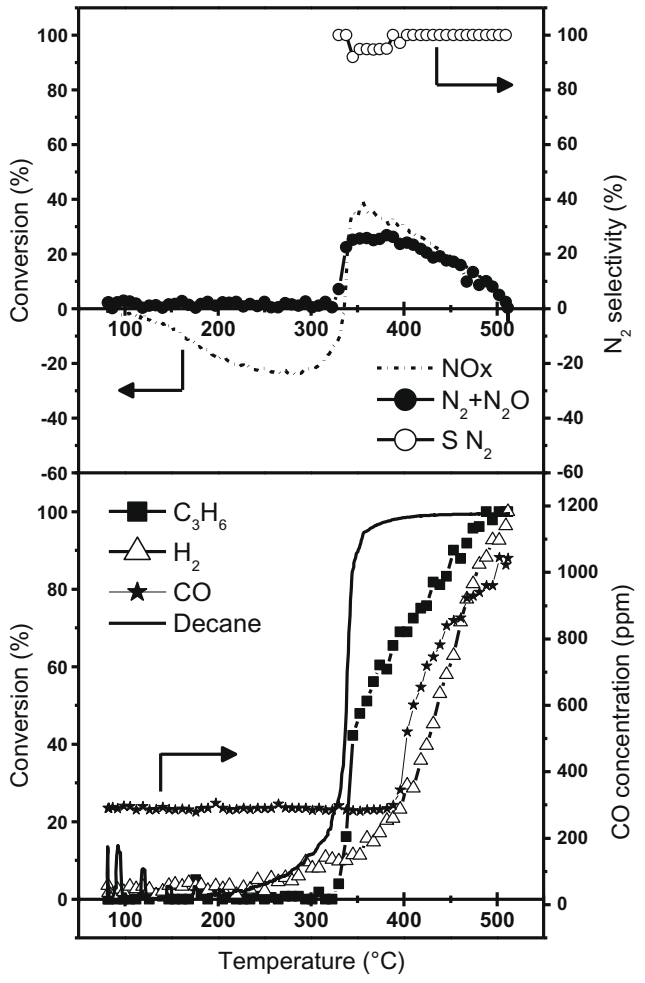

Fig. 9. Temperature-programmed reduction of NO by hydrocarbons (TPR1) on 23-Ag/Al_2O_3 (reaction conditions: 300 ppm NO, 300 ppm CO 900 ppmC C_3H_6, 1000 ppmC Décane, 2000 ppm H_2, 10 vol.% O_2, 10 vol.% CO_2, 5 vol.% H_2O – $W/F_0 = 0.072$ g s cm^{-3}).

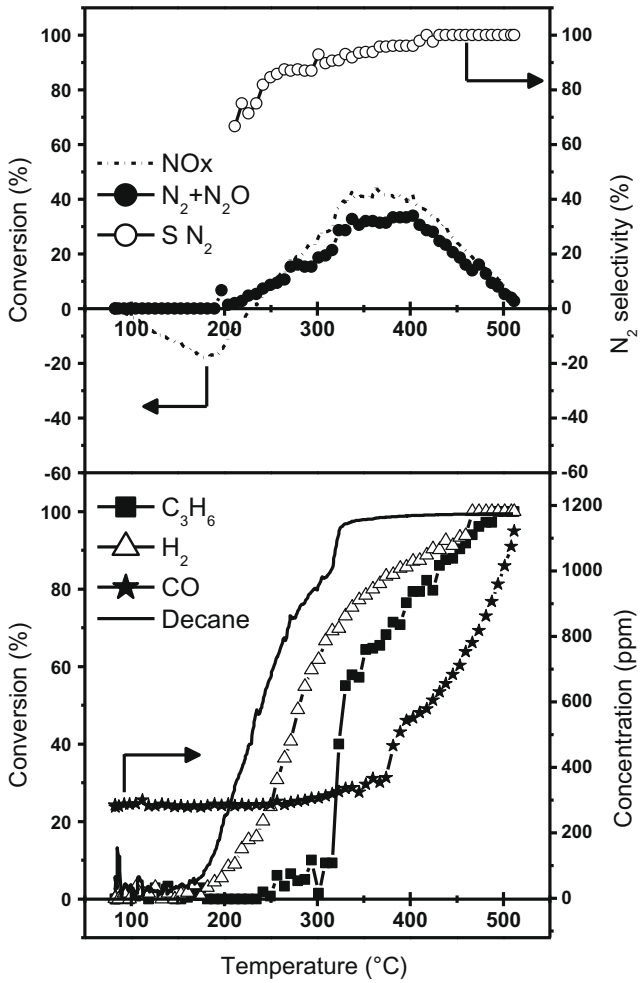

Fig. 10. Temperature-programmed reduction of NO by hydrocarbons (TPR2) on 23-Ag/Al_2O_3 (reaction conditions: 300 ppm NO, 300 ppm CO 900 ppmC C_3H_6, 1000 ppmC Decane, 2000 ppm H_2, 10 vol.% O_2, 10 vol.% CO_2, 5 vol.% H_2O – $W/F_0 = 0.072$ g s cm^{-3}).

show significant divergence in the temperature range 345–500 °C which could be ascribed to an extra formation of ad-NO_x species trapped at the surface and/or of HNO_3. Regarding the conversion of the reducing agents, it is worthwhile to note that the conversion of decane predominates at low temperature with a light-off temperature T_{50} = 338 °C. In contrast to previous observations on as-prepared 13-Ag/Al_2O_3, the conversion profile of hydrogen shifts to higher temperature with T_{50} = 439 °C whereas the conversion of propene takes place at intermediate temperatures starting above 338 °C. Probably, the most significant information is related to an extra formation of CO above 380 °C which has not been previously observed on 13-Ag/Al_2O_3.

The same agreement between NO conversion calculated on the basis of data from gas chromatography and chemiluminescence is observed in Fig. 10 which do not reveal possible enhancement of the oxidative properties of Ag at the expense of the reductive ones. On the other hand, the conversion of NO to N_2 and N_2O broadens in the temperature range 220–500 °C with a maximum NO conversion at 32 ± 2% between 323 and 424 °C. N_2 is essentially formed with low amounts of N_2O at low temperature and low conversion. Both experiments seem to be in relatively good agreement for concluding a beneficial effect of thermal aging on the conversion of NO and a slight detrimental effect on the selectivity toward the production of N_2 relative to the fresh catalyst performances. Regarding the conversion of the reducing agent, the following activity sequence can be established on the basis of the light-off temperature: $C_{10}H_{22}$ (T_{50} = 241 °C) > H_2 (T_{50} = 286 °C) > C_3H_6 (T_{50} = 330 °C) which emphasizes the fact that decane could be involved in the selective reduction of NO_x to nitrogen rather than H_2 and propene based on the comparison with Fig. 9. This observation seems to be in rather agreement with previous investigation showing that the direct NO/H_2 reaction does not occur on silver-based catalysts [33]

Catalytic behavior of the 25-Ag/Al_2O_3 catalyst is very close to that of 23-Ag/Al_2O_3. As in the case of 23-Ag/Al_2O_3, the 25-Ag/Al_2O_3 catalyst converts NO at higher temperature than 13-Ag/Al_2O_3. The maximum NO conversion (35–37%) is higher than that obtained for 23-Ag/Al_2O_3 in accordance with the higher silver loadings but it was reached in the same range of temperature with it. It is worthwhile to note that NO is selectively converted into N_2, with the same selectivities as 23-Ag/Al_2O_3 that might be a very good evidence of the similarity of the active centers in the two catalysts. Also, no change in the activity sequence on the basis of the light-off temperature has been observed after the increase of the silver loading: $C_{10}H_{22}$ (T_{50} = 242 °C) > H_2 (T_{50} = 284 °C) > C_3H_6 (T_{50} = 334 °C). This is a very important advantage of the preparation methodology using the colloid precursor. An increased loading corresponds to a higher concentration of the active centers keeping the metal particles at the same size. It is thus a very efficient route to increase the catalyst productivity for the same level of selectivity.

3.3. Tentative correlations between active silver species and catalytic behavior

As previously mentioned, one of the objectives of this study was to probe the impact of novel synthesis routes for obtaining embedded Ag/Al_2O_3 catalysts combining colloid and sol–gel methods on the catalytic performances as well as their stability under real exhaust gas conditions. Particular attention has been paid to the influence of thermal aging on the catalytic performances in the reduction of NO by hydrocarbons at high temperature under reactive conditions in order to examine the resistance to deactivation and/or, conversely, the occurrence of activation processes which might occur at high temperatures depending on the extent of surface reconstructions. Currently, surface restructuration occurs on silver-based catalysts which induce a beneficial effect on the conversion of NO to nitrogen [22,23] associated with the presence of water. In fact, water may act differently with a usual reversible inhibiting effect. However, a gradual increase with time usually occurs under wet atmosphere. The phenomena which might govern such rate enhancement are not clearly elucidated because the contribution of several processes is often difficult to separate for further quantification. By way of illustration, it is usually difficult to separate the influence of particle size and surface Ag^0/Ag^+ composition on the catalytic performance. As previously seen, the silver loading induces significant changes in the textural and structural properties of embedded Ag/Al_2O_3 catalysts with silver nanoparticles localized in different coordinative sites than those stabilized in the native alumina support (tetragonal vs. hexagonal sites on bare alumina in agreement with NMR measurements). Hence, it is expected that those modifications are governed by geometrical factors likely associated with the size and the morphology of silver particles. As suggested by XPS analysis, changes in the electronic properties of silver clusters on 13-Ag/Al_2O_3 and 23-Ag/Al_2O_3 are not evident. It seems obvious that silver retains a metallic character which is preserved during the thermal treatment. Also, neither a sintering nor a bulk oxidation process seems to occur which would express a detrimental effect on the catalytic behavior particularly on 23-Ag/Al_2O_3. Tentative comparison can be achieved between the average Ag size (d_{Ag}) roughly calculated from XPS on the basis of the Kerkhof and Moulijn model [34] previously developed for particles dispersed on porous materials. According to the model, the catalyst consists of sheets of support with cubic Pd crystallites with dimension d_{Ag} in between. It is assumed that electrons leave the sample only in a direction perpendicular to the surface and that a Lambert–Beer type law is valid for such calculations. Table 3 shows that the estimated particle size (d_{Ag}) obtained through this calculation on as-prepared and aged catalysis are comparable. However, they do not correspond to the same catalytic properties toward NO reduction to nitrogen. It seems obvious that the catalytic performance strongly depend on the operating conditions of the synthesis route but weakly on the resulting particle size of silver which are quite similar on 13-Ag/Al_2O_3 and 23-Ag/Al_2O_3 according to the margin of error.

XAES measurements are more sensitive to the chemical environment we can conclude the population of the Ag^+ species is higher for 23-Ag/Al_2O_3 which could partly explain the significant changes observed between 13-Ag/Al_2O_3 and 23-Ag/Al_2O_3, the former catalyst being quite inactive toward the transformation of NO to nitrogen contrarily to the later one.

Table 3
Comparison between of average particles size of silver from XPS according to the Kerkov–Moulijn model and catalytic performances.

Catalyst	XPS analysis	Catalytic features[a]	I_{Ag3d}/I_{Al2p}	d_{Ag}[b]	X_{NO} (%) S_{N_2} (%)
13-Ag/Al_2O_3	Fresh	0.0848	54	10.0	73.0
	Aged	0.0808	58	3.0	21.5
23-Ag/Al_2O_3	Fresh	0.0755	64	26.0	97.0
	Aged	0.0734	66	32.0	93.0

[a] Estimate of the Ag particle size, nm.
[b] From TPR experiment at $T = 300$ °C.

Returning to previous catalytic features characterizing 13-Ag/Al_2O_3 and 23-Ag/Al_2O_3, it seems obvious that they behave differently with 13-Ag/Al_2O_3 exhibiting the lowest activity in the conversion of NO and a loss of its oxidative properties after thermal aging. Conversely, the as-prepared 23-Ag/Al_2O_3 selectively converts NO to N_2, and subsequent thermal aging leads to an enhancement of the conversion of NO and a slight alteration of the selectivity with the appearance of a low amount of N_2O essentially at low conversion. As a matter of fact, the balance between Ag^0/Ag^+ probably draw the catalytic performance as previously stated [30]. According to previous explanation, the oxidation of NO to NO_2 has often been suggested as rate determining for the SCR of NO_x by hydrocarbons over alumina-based catalysts. It is well accepted that the pre-activation thermal treatment might alter the rate of NO_2 production. This reaction is currently associated with the presence of metallic particles. On the contrary, the presence of oxidic silver species do not play a key role in the NO/O_2 reaction. Hence, an optimal surface Ag^0/Ag^+ is needed for catalyzing the conversion of NO to nitrogen. It seems obvious that this condition is not fulfilled on 13-Ag/Al_2O_3 because of the greater extent of Ag^0, and subsequent thermal aging leads also to a detrimental effect on the oxidative properties of this catalyst which is probably not correlated to the formation of well-dispersed electrophilic silver species. On the contrary, the balance between Ag^0 and Ag^+ species seems to be more favorable on freshly-prepared 23-Ag/Al_2O_3. This Ag^0/Ag^+ ratio would not depend on the particle size but seems to be sensitive to the operating conditions during the synthesis route. The presence of chemisorbed N species after aging on 23-Ag/Al_2O_3 by XPS highlights the presence of zero-valent silver which promotes the dissociation pathway of NO. Such an observation agrees with the fact that the coexistence of Ag^0 and Ag^+ is needed for promoting the reduction of NO_x but in an optimal value to obtain selectively nitrogen. In this sense, the determining role of hydrogen earlier mentioned [35,36] is in this present study well-illustrated, partly preserving the presence of metallic silver species particularly on 23-Ag/Al_2O_3. In fact, a greater extent of dissociative adsorption of oxygen on Ag^0 which would favor the production of NO_2 on aged 23-Ag/Al_2O_3 might also explain the rate enhancement in NO conversion to nitrogen [36]. In parallel reaction pathways involved on Ag^0 leading to the formation of N_2O will also be enhanced.

An outstanding observation is also related to the detection of CO on 23-Ag/Al_2O_3 which underlines the occurrence of reforming reactions as previously reported. It has been earlier suggested that the production of significant amount of CO characterizes the catalyst acidity [26]. By way of illustration, it was earlier found that the reduction of nitrogen dioxide by propene on H-mordenite leads to the production of $N_2/CO/CO_2$ in the ratio 1/1/2. The examination of Figs. 9 and 10 rules out this hypothesis because alumina is much less acidic than zeolithe. However, the possible stabilization of nitrosonium ions assisted by the acidic properties of alumina capable to react rapidly with surface oxide ions and oxygen to yield adsorbed nitrate species could contribute to a better activity. Alternately, the formation of CO can be ascribed to the involvement of partial oxidation and/or reforming reactions in accordance with earlier investigations [36–38]. The reverse Water–Gas-Shift reaction might also contribute in our operating conditions. The lack of observation of subsequent hydrogen formation on 23-Ag/Al_2O_3 probably reflects its high reactivity under lean conditions and could be related to the beneficial effect observed on the conversion of NO over 23-Ag/Al_2O_3. Satokawa et al. [38] have already reported the beneficial effect of hydrogen on the conversion of NO by light hydrocarbons. However, further explanations on the origin of such an effect are

desirable because two different viewpoints compete. The first one being associated with the impact of hydrogen on the oxidation state of silver and on structural aspects associated with the stabilization of small Ag clusters due to subsequent coalescence of isolated Ag^+ species, while the second one is mostly related to the nature of adsorbates. As a matter of fact, both aspects could be reconciled according to Burch et al. [21] who suggested two different reaction pathways according to the nature of the silver species. On metallic Ag^0 species, the competition between oxidative and reductive reaction will be in favor of the former which considerably limits the conversion of NO. Additionally, it would proceed via its dissociation which differs from $Ag_n^{\delta+}$ clusters where NO can be selectively transformed into nitrogen. Now returning to our catalytic observations, particularly on aged catalysts, our catalytic features could be correctly explained on the basis of the above-mentioned mechanism proposal which accounts for the relative distribution of $Ag^0/Ag^{\delta+}$ in explaining the selectivity behavior [39]. Hence, the formation of N_2O on the as-prepared 13-Ag/Al_2O_3 contrary to 23-Ag/Al_2O_3 would suggest a relatively higher concentration of Ag^0 on the former catalysts. As shown, the reverse tendency characterizes the as-prepared 23-Ag/Al_2O_3. However, the slow formation of N_2O after aging signifies a shift of the Ag^0/Ag^+ to a preferential formation of Ag^0 which could not be formally associated with the involvement of coalescence processes as earlier proposed by Satokawa et al. [38] according to our XPS observations.

4. Conclusions

The characterization of the catalysts prepared via embedding the pre-prepared silver colloids into the alumina via a sol–gel procedure indicated the colloids preserved their size and oxidation state. However, as XAES demonstrates, the catalysts prepared in a sol–gel with a lower amount of water led to embedded colloids with a higher population of Ag^+ species. The catalytic behavior of the resultant catalysts was well correlated with the concentration of these species and the particle size. Thus, the active silver species of the 23-Ag/Al_2O_3 catalysts selectively converts NO to N_2, and subsequent thermal aging leads to an enhancement of the conversion of NO and only a slight alteration of the selectivity with the appearance of low amounts of N_2O assigned to slight changes on the surface Ag^0/Ag^+ ratio.

Acknowledgments

Vasile I. Pârvulescu thanks ANCS for funding the project 21048/1997. Ryan Richards would like to thank the Colorado School of Mines for financial support. The authors thank Kostas Tryandafylidis for fruitful discussions.

References

[1] (a) M. Bron, D. Teschner, A. Knop-Gericke, F. Jentoft, J. Kroehnert, J. Hohmeyer, C. Volckmar, B. Steinhauer, R. Schlogl, P. Claus, Phys. Chem. Chem. Phys. 9 (2007) 3559–3569;
(b) M. Steffan, A. Jakob, P. Claus, H. Lang, Catal. Commun. 10 (2009) 437–441.
[2] (a) T. Mitsudome, S. Arita, H. Mori, T. Mizugaki, K. Jitsukawa, K. Kaneda, Angew. Chem. Int. Ed. 47 (2008) 7938–7940;
(b) D.P. Debecker, C. Faure, M.-E. Meyre, A. Derre, E.M. Gaigneaux, Small 4 (2008) 1806–1812.
[3] (a) T. Sato, S. Goto, Q. Tang, S. Yin, J. Mater. Sci. 43 (2008) 2247–2253;
(b) K. Eränen, F. Klingstedt, K. Arve, L-E. Lindfors, D.Y. Murzin, J. Catal. 227 (2004) 328–343;
(c) N. Jagtap, S.B. Umbarkar, P. Miquel, P. Granger, M.K. Dongare, Appl. Catal. B Environ. 90 (2009) 416–425.
[4] N. Severin, S. Kirstein, I.M. Sokolov, J.P. Rabe, Nano Lett. 9 (2009) 457–461.
[5] C. Zhang, P. Chen, J. Liu, Y. Zhang, W. Shen, H. Xu, Y. Tang, Chem. Commun. 28 (2008) 3290–3292.
[6] T. Mitsudome, Y. Mikami, H. Funai, T. Mizugaki, K. Jitsukawa, K. Kaneda, Angew. Chem. Int. Ed. 47 (2008) 138–141.
[7] M. Muniz-Miranda, J. Raman Spectrosc. 35 (2004) 839–842.
[8] M. Bron, D. Teschner, A. Knop-Gericke, B. Steinhauer, A. Scheybal, M. Haevecker, D. Wang, R. Foedisch, D. Hoenicke, A. Wootsch, R. Schlogl, P. Claus, J. Catal. 234 (2005) 37–47.
[9] Z.-J. Jiang, C.-Y. Liu, L.-W. Sun, J. Phys. Chem. B 109 (2005) 1730–1735.
[10] H. Zhao, J. Zhou, H. Luo, C. Zeng, D. Li, Y. Liu, Catal. Lett. 108 (2006) 49–54.
[11] Y. Lu, Y. Mei, M. Drechsler, M. Ballauff, Angew. Chem. Int. Ed. 45 (2006) 813–816.
[12] P.G.N. Mertens, F. Cuypers, P. Vandezande, X. Ye, F. Verpoort, I.F.J. Vankelecom, D.E. De Vos, Appl. Catal. A Gen. 325 (2007) 130–139.
[13] (a) M.J. Lippits, A.C. Gluhoi, B.E. Nieuwenhuys, Top. Catal. 44 (2007) 159–165;
(b) L. Zhang, C. Zhang, H. He, J. Catal. 261 (2009) 101–109;
(c) A. Musi, P. Massiani, D. Brouri, J.-M. Trichard, P. Da Costa, Catal. Lett. 128 (2009) 25–30.
[14] Y.-C. Kim, N.-C. Park, J.-S. Shin, S.R. Lee, Y.J. Lee, D.J. Moon, Catal. Today 87 (2003) 153–162.
[15] A. Iglesias-Juez, M. Fernandez-Garcia, A. Martinez-Arias, Z. Schay, Zs. Koppany, A.B. Hungria, A. Fuerte, J.A. Anderson, J. Conesa, J. Soria, Top. Catal. 30/31 (2004) 65–70.
[16] M. Richter, U. Bentrup, R. Eckelt, M. Schneider, M.-M. Pohl, M.-M.R. Fricke, Appl. Catal. B Environ. 51 (2004) 261–274.
[17] K. Arve, F. Klingstedt, K. Eranen, D. Yu Murzin, L. Capek, J. Dedecek, Z. Sobalik, B. Wichterlova, K. Svennerberg, L.R. Wallenberg, J.-O. Bovin, J. Nanosci. Nanotechnol. 6 (2006) 1076–1083.
[18] K. Arve, K. Svennerberg, F. Klingstedt, K. Eraenen, L.R. Wallenberg, J.-O. Bovin, L. Capek, D.Yu. Murzin, J. Phys. Chem. B 110 (2006) 420–427.
[19] R. Burch, J.P. Breen, C.J. Hill, B. Krutzsch, B. Konrad, E. Jobson, L. Cider, K. Eraenen, F. Klingstedt, L.-E. Lindfors, Top. Catal. 30/31 (2004) 19–25.
[20] J.P. Breen, R. Burch, C. Hardacre, C.J. Hill, J. Phys. Chem. B 109 (2005) 4805–4807.
[21] R. Burch, J.P. Breen, F.C. Meunier, Appl. Catal. B Environ. 39 (2002) 283–303.
[22] K. Shimidzu, A. Satsuma, T. Hattori, Appl. Catal. B 25 (2000) 239–247.
[23] F.C. Meunier, R. Ukropec, C. Stapleton, J.R.H. Ross, Appl. Catal. B 30 (2001) 163–172.
[24] D. Massiot, F. Fayon, M. Capron, I. King, S. Le Calvé, B. Alonso, J.-O. Durand, B. Bujoli, Z. Gan, G. Hoatson, Magn. Reson. Chem. 40 (2002) 70–76.
[25] (a) D. Freude, J. Karger, Handbook of Porous Solids, vol. 1, Wiley-VCH, Weinheim, Germany, 2002, pp. 465–504;
(b) G. Crépeau, V. Montouillout, A. Vimont, L. Mariey, T. Cseri, F. Maugé, J. Phys. Chem. B 110 (2006) 15172–15185.
[26] T. Gerlach, U. Ullgen, M. Burtoszek, M. Baerns, Appl. Catal. B 22 (1999) 269–278.
[27] S.W. Gaarenstoom, N. Winograd, J. Chem. Phys. 67 (1977) 3500–3506.
[28] M.T. Anthony, M.P. Seah, Surf. Interface Anal. 6 (1984) 95–106.
[29] P. Sazama, L. Čapek, H. Drobná, Z. Sobalík, J. Dedecek, K. Arve, B. Wichterlová, J. Catal. 232 (2005) 302–317.
[30] N. Bogdanchikova, F.C. Meunier, M. Avalos-Borja, J.P. Breen, A. Pestryakov, Appl. Catal. B 36 (2002) 287–297.
[31] W.L. Dai, Y. Cao, L.P. Ren, X.L. Yang, J.H. Xu, H.X. Li, H.Y. He, K.N. Fan, J. Catal. 228 (2004) 80–91.
[32] (a) D. Briggs, M.P. Seah, Practical Surface Analysis, second ed., vol. 1, John Wiley, Chichester, 1999;
(b) A.S. Mamede, G. Leclercq, E. Payen, P. Granger, L. Gengembre, J. Grimblot, Surf. Interface Anal. 34 (2002) 105–111.
[33] K. Eranen, F. Klingstedt, K. Arve, L.E. Lindfors, D.Y. Murzin, J. Catal. 227 (2004) 328–343.
[34] F.P.J.M. Kerkhof, J.A. Moulijn, J. Phys. Chem. 83 (1979) 1612–1619.
[35] M. Richter, U. Bentrup, R. Eckelt, M. Shneider, M.M. Pohl, R. Frike, Appl. Catal. B 51 (2004) 261–274.
[36] N. Jagtap, S.B. Umbarkar, P. Miquel, P. Granger, M. Dongare, Appl. Catal. B Environ. 90 (2009) 416–425.
[37] (a) Y. Kuroda, T. Mori, H. Sugiyama, Y. Uozumi, K. Ikeda, A. Itadani, M. Nagao, J. Colloid Interface Sci. 333 (2009) 294–299;
(b) J.T. Ranney, S.R. Bare, John L. Gland, Catal. Lett. 48 (1997) 25–29.
[38] (a) S. Satokawa, Chem. Lett. 29 (2000) 294–295;
(b) S. Satokawa, J. Shibata, K. Shimizu, A. Satsuma, T. Hattori, Appl. Catal. B Environ. 42 (2003) 179–186.
[39] A. Iglesias-Juez, A.B. Hungria, A. Martinez-Arias, A. Fuerte, M. Fernandez-Garcia, J.A. Anderson, J.C. Conesa, J. Soria, J. Catal. 217 (2003) 310–323.